Long-time self-diffusion of spherical colloidal particles measured with fluorescence recovery after photobleaching

A. van Blaaderen
Van't Hoff Laboratory, University of Utrecht, Padualaan 8, 3584 CH Utrecht, The Netherlands

J. Peetermans and G. Maret
Hochfeld Magnetlabor, Max Planck Institut für Festkörperforschung, 166x, F-38042 Grenoble Cedex, France

J. K. G. Dhont
Van't Hoff Laboratory, University of Utrecht, Padualaan 8, 3584 CH Utrecht, The Netherlands

(Received 23 October 1991; accepted 15 November 1991)

Long-time self-diffusion coefficients in concentrated colloidal dispersions of silica spheres, with various interaction potentials, were measured with the fluorescence recovery after photobleaching technique. Charge stabilized spheres were measured in solutions of LiCl in dimethylformamide with varying ionic strength. Sterically stabilized hard-sphere-like stearyl silica dispersions were studied in cyclohexane. The fluorophore used, fluorescein-isothiocyanate, was covalently attached to the surface of the spheres (for the charged particles) or buried inside the silica core (for the hard spheres). The particles were characterized by electrophoresis, static and dynamic light scattering, and transmission electron microscopy. The experimental results are discussed and compared with existing theories on long-time self-diffusion.

I. INTRODUCTION

The simplest quantity describing the motion of a Brownian particle is its mean square displacement (msd) as a function of time. For independent colloidal particles the msd resulting from many impacts of solvent molecules, is a linear function of time, characterized by the single particle diffusion coefficient D_0, whose value is given by the Stokes–Einstein relation.[1] At higher concentrations direct interactions [(screened) Coulombic, van der Waals and/or steric forces] and hydrodynamic interactions will influence the msd. In the limit that a particle has moved a distance in which it interacted with many other Brownian particles, the msd is again linear with time. The proportionality constant is now called the long-time self-diffusion coefficient D_S^L. Since the long-time self-diffusion coefficients D_S^L relates to single particle dynamics, one has to tag individual particles in some way in order to measure it. In its simplest form this was already done by Perrin in 1910 when he determined Avogadro's number by measuring the msd of tagged particles through a microscope.[2]

Most experimental information about the dynamics of colloids is presently obtained with dynamic light scattering (DLS). With DLS the decay rate of density fluctuations is measured. The angle of observation determines the wave number of the Fourier component of the fluctuating particle density of which the time dependence is recorded. However, in order to measure D_S^L, it is necessary to make a dispersion of many refractive index matched host particles together with a few strongly scattering tracer particles. Although different in scattering properties, the tracer and the host particles must interact through the same forces. The requirements for D_S^L measurements with DLS have only been met for sterically stabilized particles in apolar solvents.[3–5] These particles interact more or less as hard spheres. It is also possible to measure D_S^L with DLS by using the polydispersity in scattering properties of individual particles.[6] If however, there is also a polydispersity in size, the theoretical interpretation of experimental data becomes quite cumbersome.

To our knowledge, no D_S^L results of charged systems have been reported, as measured with DLS, because of difficulties with the matching procedure (see, however, Ref.7). There are a number of other techniques that, in principle, enable the measurement of D_S^L for colloidal particles: dynamic neutron scattering, field gradient spin echo NMR, forced Rayleigh scattering (FRS, also called holographic relaxation spectroscopy) and fluorescence recovery after photobleaching (FRAP, also called fringe pattern photobleaching). With these techniques, D_S^L as a function of volume fraction, as far as we know, is only reported for charged particles with FRS.[8] Gorti *et al.* measured D_S^L with FRAP of charged particles as a function of the ionic strength at a given volume fraction of Brownian particles.[9] FRS and FRAP are closely related techniques and measure self-diffusion through the disappearance of an optically created fringe pattern of tagged particles in the dispersion.

In this paper we report on FRAP measurements of D_S^L, as a function of the volume fraction of Brownian particles, and for various interaction potentials. Use has been made of well characterized model silica spheres, either charge stabilized in dimethylformamide (DMF) or sterically stabilized through a short n-18 alkane in cyclohexane. The fluorescence photobleaching characteristics were obtained through the dye fluoresceinisothiocyanate (FITC). The FITC labels are covalently attached to the surface and inside the core of the silica spheres through a silane coupling agent. For the silica particles dispersed in DMF the FITC molecules are chemically attached to the particle surface and are partly

 0021-9606/92/064591-13$06.00

responsible for the stabilizing negative charge on the spheres through the dissociation of the carboxylic groups on FITC. The hard sphere particles in cyclohexane do not have any FITC molecules on their surface. Here the FITC is buried inside the particle core and is shielded from the surface by a 10 nm thick layer of pure silica and the surface coating of octadecanol. Details of the synthesis and characterization will be presented elsewhere.[10]

In the next section we shortly discuss the relevant interaction potentials for the systems studied and the different time scales important for an understanding of several diffusion properties of interacting particles. Also the FRAP technique is discussed in some detail. In Sec. III we describe and discuss the experimental procedure of particle synthesis and characterization. Section IV contains the long-time self-diffusion results together with details about the FRAP experiments. A detailed quantitative analysis of the data is given in Sec. V. Finally, Sec. VI contains some concluding remarks.

II. THEORY

A. Interaction forces

In the following we consider a monodisperse colloidal system of homogeneous spheres of radius a at a temperature T. The *negatively charged* silica spheres are suspended in a solution of LiCl in DMF. We use the well known DLVO potential to describe the direct interactions between two particles at a center to center distance r,[11]

$$V(r) = V_R(r) + V_A(r), \tag{1}$$

where the double-layer repulsion is given in S.I. units by

$$V_R(r) = 2\pi\epsilon a\psi_0^2 \ln\{1 + \exp[-\kappa(r-2a)]\}, \tag{2}$$

and the van der Waals attraction is

$$V_A(r) = -\frac{A}{6}\left[\frac{2a^2}{r^2-2a^2} + \frac{2a^2}{r^2} + \ln\left(\frac{r^2-4a^2}{r^2}\right)\right]. \tag{3}$$

The constants appearing in Eqs. (2) and (3) are the permittivity of DMF ϵ, the particle surface potential ψ_0, the Hamaker constant A, for silica dispersed in DMF, and the inverse Debye screening length

$$\kappa = e\left(\frac{2cN_a}{\epsilon kT}\right)^{1/2}, \tag{4}$$

with e the absolute value of the electronic charge, c the molar concentration of LiCl, N_a Avogadro's number, and k the Boltzmann constant.

Within the approximation of the double layer repulsion Eq. (2), the surface charge can be approximated by,[12]

$$Q = 4\pi\epsilon\frac{kT}{e}\kappa a^2\left\{2\sinh(\psi/2) + \frac{4}{\kappa a}\tanh(\psi/4)\right\}, \tag{5}$$

with $\psi = \psi_0 e/kT$.

The *sterically stabilized* silica spheres in cyclohexane experience the van der Waals attraction, approximated by Eq. (3), and a short range repulsion due to the short alkane chains on the surface of the spheres. However, the mean refractive index of the silica particles ($n_p = 1.45$) is very close to that of cyclohexane ($n_s = 1.43$). As a consequence the Hamaker constant is relatively small. The same holds for the Hamaker constant for the particles in DMF ($n_s = 1.43$). We refer to Ref. 13 for an approximate calculation of the Hamaker constant, where the sterically stabilizing alkane layer is also taken into account. For good solvents, like cyclohexane, the interaction between the short layers of alkane molecules is repulsive. This makes a hard sphere potential a very good approximation to describe the interactions, as has been shown in many experiments.[14–16]

B. Self-diffusion

As a consequence of the large mass and size difference between a colloidal particle and a solvent molecule, it suffices in the description of the dynamics of these particles to represent the molecular motions only in an "average way." In this description the effect of the suspension medium appears only through friction factors of the colloidal particle with the solvent. For a single spherical colloidal particle, with stick boundary conditions, in a Newtonian fluid, the friction factor is given by Stokes expression

$$f = 6\pi\eta a, \tag{6}$$

where η is the shear viscosity of the solvent.

Another consequence of the large particle mass is that its velocity fluctuates on a "Brownian time scale" τ_B, on which the colloid itself moves only over a small fraction of its radius. The Brownian time is given by

$$\tau_B = \frac{m}{f}, \tag{7}$$

with m the particle mass. For time scales $\gg\tau_B$, particle velocities are completely relaxed and the particle will move in a diffusive way. That is, for one-dimensional displacements, the mean square displacement at time t, $\langle x^2(t)\rangle$, is given by

$$\langle x^2(t)\rangle = 2D_0 t, \quad t \gg \tau_B. \tag{8}$$

Einstein was the first to derive the connection between the diffusion coefficient D_0 and the friction factor,[1]

$$D_0 = \frac{kT}{f}. \tag{9}$$

Relations (8) and (9) are valid for noninteracting particles. Things are more complicated for interacting particles. The msd is influenced by both direct interactions (Sec. II A) and hydrodynamic interactions. A moving particle creates a velocity field in the fluid that can induce a force on particles surrounding it. An estimate of the time τ_H it takes such a viscous shear wave or hydrodynamic interaction to travel between particles is[17]

$$\tau_H = n^{-2/3}\frac{\rho}{\eta}, \tag{10}$$

with n the particle number density and ρ the mass density of the suspension medium. For moderate concentrated suspensions the inter particle distance, $n^{-1/3}$, is of the order of the particle radius. This makes τ_H of the same order as τ_B meaning that for times $\gg\tau_B$ hydrodynamic interactions can be considered as acting instantaneously.

The time required for a particle to diffuse over a typical inter particle interaction distance ξ results in yet another characteristic time τ_I,

$$\tau_I = \frac{\xi^2}{D_0}. \tag{11}$$

For times $\tau_H \ll t \ll \tau_I$ the particle diffuses in an approximately constant configuration of the other particles and its msd is only influenced by hydrodynamic interactions. The displacements due to drift velocities induced by the direct interaction forces, can be neglected for these times. In general the short-time self-diffusion coefficient D_S^S characterizes the particle displacements for these short times

$$\langle x^2(t)\rangle = 2D_S^S t, \quad \tau_B \ll t \ll \tau_I. \tag{12}$$

For hard spheres Beenakker and Mazur[18] have been able to evaluate D_S^S over a large range of volume fractions by a resummation procedure of all hydrodynamic contributions. Their results are in good agreement with experimental results on D_S^S.[19]

On larger time scales, $\geqslant \tau_I$ the theoretical description becomes more complicated, because changes in neighboring particle configurations have to be taken into account. A particle moving over distances ξ in a concentrated dispersion will encounter other particles, slowing down the diffusion. In this regime the msd is not linear with time. After many collisions with other Brownian particles, the effects of the direct inter particle forces are experienced in an averaged way, again resulting in diffusive motion, characterized by the "long-time self-diffusion coefficient" D_S^L,

$$\langle x^2(t)\rangle = 2D_S^L t, \quad t \gg \tau_I. \tag{13}$$

The theoretical progress in calculating D_S^L is less than for D_S^S. A first order in the volume fraction calculation, including hydrodynamic interactions, has been performed for hard spheres by Batchelor and later by Cichocki and Felderhof (see Ref. 20 and references therein)

$$D_S^L = D_0(1 - 2.0972\phi), \tag{14}$$

where ϕ is the volume fraction of the hard spheres.

The first order in ϕ coefficient consists of two parts. One describes the hydrodynamic slowing down of the tracer particle in an equilibrium configuration of the other particles. This contribution equals D_S^S; for hard spheres with stick boundary conditions its value is -1.8315. There is also a long-time contribution due to the modification of the pair distribution function of the interacting spheres: the "cage" effect. Hydrodynamics contributes significantly to this part: Without hydrodynamics its value is -2 for hard spheres,[21] while including hydrodynamics results to a reduction of this contribution to -0.2657.

Although the extension to calculate the first order term in ϕ for other interaction potentials is straightforward, along the lines given by Cichocki and Felderhof,[20] it is instructive to consider a simplified way to describe the effects of a repulsive part in the interaction potential on D_S^L.[22] The whole effect of the repulsion is now described by an increased effective hard sphere interaction radius b, while the hydrodynamic radius is still given by the true hard-core radius a, with $a < b$. For $b/a \approx 1.3$ the coefficient in Eq. (14), with the volume fraction as calculated from the radius b, becomes -1.26, while for $b/a \approx 8$ it is -1.74, still significantly *larger than* -2.10.[22] Physically, this means that for highly charged particles hydrodynamics becomes unimportant for the D_S^S part of D_S^L but remains important for the distortion of the equilibrium structure, and thereby significantly affects D_S^L.

Quantitative theoretical predictions at higher volume fractions are scarce. Brownian dynamic simulations for charged spheres have been performed using semiempirical two-particle mobility tensors to include hydrodynamic interactions.[23] Results were calculated for high and low ionic strength as a function of the volume fraction. The volume fractions were also scaled with respect to an effective hard-core radius b, where b was determined such that it gave approximately the same thermodynamic excess properties as a hard sphere system with the corresponding volume fraction. To make a comparison with the results to first order in ϕ as given by Cichocki and Felderhof,[22] the high ionic strength system was characterized by an $b/a \approx 1.2$, while the low ionic strength system gave $b/a \approx 1.7$. As would be expected, the direct interactions caused a clear decrease of D_S^L at the same ϕ for increasing repulsion. At the same time D_S^S increased towards D_0. However, the system where $b/a \approx 1.7$, hardly showed any dependence of D_S^L on hydrodynamics and the $b/a \approx 1.2$ case showed only a small decrease of D_S^L if hydrodynamics was included. These results contradict the (exact) low order ϕ results, but it is not clear to what extent this is caused by the higher order interactions or the use of the semiempirical two-body hydrodynamics description.

By extending the Brownian dynamics scheme to hard spheres, Cichocki and Hinsen were able to simulate the dynamics of hard spheres without hydrodynamic interactions. From the msd they obtained D_S^L for several volume fractions up to $\phi = 0.5$.[24] These data can be used to calculate D_S^L with hydrodynamics by a recent proposal of Medina-Noyola.[25] He suggests, as a first approximation for self-diffusion at high volume fractions, to decouple the hydrodynamic effects from the direct interactions, or formally

$$D_S^L = D_S^S \cdot D_S^H / D_0, \tag{15}$$

where D_S^S is, again, the short-time self-diffusion coefficient taking the hydrodynamic interactions into account, and D_S^H is the long-time self-diffusion coefficient in the absence of hydrodynamic interactions.

At low ϕ the assumptions made by Medina-Noyola turn out to give erroneous results. The predicted first order in ϕ coefficient in Eq. (14) resulting from Eq. (15) is found to be -3.831. However, it is expected that the approximations will be better for higher volume fractions.[25]

C. Fluorescence recovery after photobleaching (FRAP)

FRAP is a conceptually simple method to measure self-diffusion. In this method the species of interest are labeled with a fluorophore. After an intense light pulse a portion of the sample is irreversibly photobleached and the motion of the particles is followed by measuring the characteristic time for the bleached region to fade away as a result of diffusion of the colloids. Originally the method was used to measure the diffusion of molecules in membranes, but recent experimental improvements have extended its use to a whole range of new systems.

These experimental improvements have been developed independently by two groups.[26,27] Although the principles are the same, experimental details differ. The setup used in our work is essentially the same as described by Davoust *et al.*[27] The most important difference is, that we do not use separate beams for reading and bleaching. This is easier to align and ensures a better stability of the position of the reading fringes with respect to the bleached fringe pattern. The experimental setup is schematically depicted in Fig. 1.

The photobleaching pattern is realized by crossing two coherent laser beams in the sample under some angle θ. The crossed beams give rise to a sinusoidal fringe pattern with spacing $L = 2\pi/q$ set by the crossing angle, $q = (4\pi/\lambda)\sin(\theta/2)$, with λ the laserlight wavelength in the dispersion. Since the smallest L possible is close to 1 μm, the FRAP method provides for almost all colloidal systems only the long-time self-diffusion coefficient D_S^L. After bleaching, the pattern is monitored by the same fringe pattern, produced by the two beams at a very low intensity. The fluorescent signal is picked up by a glass fiber while the scattered light is filtered out. To protect the photomultiplier during the bleach pulse the high intensity signal is blocked by a shutter. Excitation and bleaching of the fluorescein groups is done with an Ar monomode laser at 488 nm stabilized with an ethalon. A typical bleach pulse ($\approx$400 mW/mm^2) has a duration of 1 s. The intensity is then attenuated to monitor the remaining fluorescence after the bleaching by means of a Pockels cell between two crossed polarizers. The fringes are spatially modulated by a sinusoidally vibrating mirror ($\approx$1 kHz). The mirror is piezoelectrically driven with a small amplitude, comparable to L, in a direction normal to its surface. The fluorescence emission of the bleached sample is now modulated, as the bleached pattern and the moving illuminating fringes fall into and out of phase; the changing fluorescence signal is obtained with lock-in detection. The switching in the setup is controlled by a microcomputer that also collects the data (see Fig. 1).

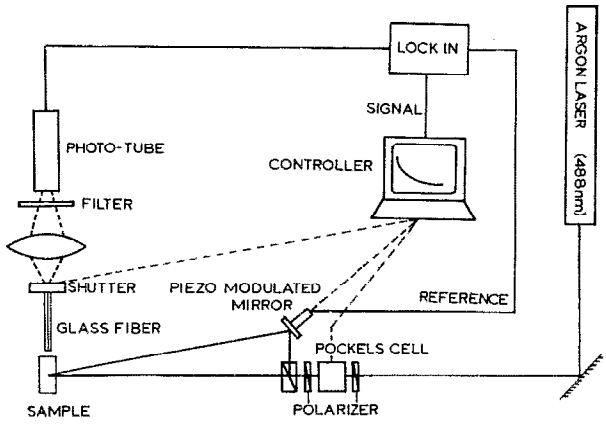

FIG. 1. Experimental setup for the fluorescence recovery after photobleaching experiments.

The time dependence of any nonuniform concentration profile $c(\mathbf{r},t)$ of fluorescent particles in a *uniform solution of other particles of the same size and with the same interaction potential*, for times $\gg \tau_I$, is described by Ficks law

$$\frac{\partial}{\partial t} c(\mathbf{r},t) = D_S^L \nabla^2 c(\mathbf{r},t) \tag{16}$$

with the bleach profile given by $c(\mathbf{r},0)$. The fluorescent intensity I_f that is measured is proportional to

$$I_f(t',t) \propto \int I(\mathbf{r},t')c(\mathbf{r},t)d\mathbf{r}, \tag{17}$$

where I is the t'-modulated reading fringe intensity. The range of integration in Eq. (17) is the illuminated region in the sample. If this range of integration is much larger than the typical Fourier wavelengths of I and c, it follows from Eq. (16) and Eq. (17) that, whenever *I and/or c* are sinusoidal functions of $\mathbf{r}$ with wave vector q, that

$$I_f(t',t) \propto A + B(t')\cdot\exp(-D_S^L q^2 t). \tag{18}$$

Here B is the product of the amplitude of the t'-modulated qth Fourier component of I and the corresponding (t'-independent) component of $c(\mathbf{r},0)$. In Eq. (18) we added a constant background intensity A, which is the result of infinite wavelength Fourier components of I and c in Eq. (17). The above-mentioned mechanically, sinusoidally vibrating mirror sets $B(t') = B_0 \sin(\omega t')$, with $\omega \approx 1$ kHz. Detecting the 1 kHz component of $I(t',t)$ by means of a lock-in amplifier than results, according to Eq. (18) in a single-exponentially decaying signal $S(t)$

$$S(t) \propto \exp(-D_S^L q^2 t). \tag{19}$$

Note that this is a way to eliminate the usually large background A in the fluorescent intensity Eq. (18). The best signal to noise ratio is obtained if *both* I and c are sinusoidal (with the same wave vector). This is established by using the attenuated bleach beams as reading beams.

Since turbidity causes no shift in the periodicity of the bleached pattern, but only a more diffuse bleach pattern, highly scattering samples can also be measured. It is possible to correct for photobleaching during the recovery phase by dividing the signal from the lock-in amplifier by the now also slowly decreasing background signal A in Eq. (18). This ratio-mode operation also corrects for changes in time of fluorescence quantum yield, laser intensity and or amplifier gains.

The use of a crossed beam interference pattern makes the FRAP method very similar to forced Rayleigh scattering. Here, instead of bleaching, molecules are excited to a state in which absorption characteristics are changed. The wavelength of the reading beam is chosen close to the maximum absorption of the excited molecules. This beam sees an optical grating slowly fading by the diffusion of the particles. The intensity in the first order diffracted beam decays again exponentially with a decay time, determined by D_S^L as in Eq. (19). The lifetime of the excited state of the fluorescent labels should be much larger than the decay time $1/D_S^L q^2$.

In contrast to the FRAP technique FRS is not very suitable for measurements in turbid samples. With turbid samples the spatial modulation depth of the fringe pattern de-

cays as a function of distance into the sample, for both techniques similarly. But in FRS the reading suffers from scattering as well, as Bragg scattering is used to detect a signal. With FRAP the scattered intensity does not reach the detector because of the cut-off filter and the lock-in detection discriminates a small signal against a strong background.

III. SYNTHESIS AND CHARACTERIZATION OF THE COLLOIDAL SYSTEMS

A. Synthesis

The synthesis of the labeled, charge and sterically stabilized silica spheres will be described in detail elsewhere.[10] Here we will only briefly describe the synthesis of these particles, and discuss their characterization.

1. Charged spheres (CS)

The core of the silica particles was made by the method developed by Stöber *et al.*[28] The monomer tetraethoxysilane is catalytically hydrolyzed by ammonia in a mixture of water and ethanol. Quite monodisperse silica spheres result from condensation reactions in which siloxane bonds are formed. In the same reaction mixture the particles were coated with the silane coupling agent γ-aminopropyltriethoxysilane (APS). A small part of these APS molecules was first covalently linked to the fluorophore fluorescein-isothiocyanate (FITC/APS, molar ratio $\approx 1/300$). The increase in radius as a result of the coating of the surface with APS and FITC molecules is of the order of a nanometer. Each colloidal particle is labeled with approximately 3000 molecules FITC. The stabilizing negative charge on the particles is not only due to the carboxylic groups on the FITC, but also originates from deprotonated silanol groups on the silica/coupling agent surface. The particles were suspended in dimethylformamide (DMF) through repeated centrifugation.

2. Hard spheres (HS)

Silica spheres, sterically stabilized with stearyl alcohol (octadecanol), were first synthesized and used as a colloidal model system by Van Helden *et al.*[16] The same esterification in a melt of stearyl alcohol at about 200 °C has been used here. The silica core particles were modified in the same way as described for the charged spheres. However, after the treatment with the coupling agent another layer of approximately 10 nm silica was deposited on the particles. The FITC molecules are then completely built into the inorganic silica matrix and are still fluorescent and bleachable. Even after the quite severe conditions of the esterification of the surface with octadecanol, the major part of the FITC molecules inside the spheres were unaffected. Because the outer layer of these particles is not different from the stearyl silica used in many studies, it was no surprise to find the same dispersion properties in various solvents. The particles were transferred to cyclohexane by centrifugation.

B. Characterization

1. Particle radii

Particle sizes were measured with transmission electron microscopy (TEM), with static light scattering (SLS) and dynamic light scattering (SLS).

The TEM micrographs were obtained using a Philips EM301 transmission electron microscope in combination with interactive image analysis (IBAS). Number average radii $\langle R \rangle$ and relative standard deviations σ were determined from image analysis using about 700 particles. Figure 2 shows a TEM picture of the charged spheres, showing that the particles are smooth and almost perfectly spherical.

Light scattering measurements were done at 25 ± 0.1 °C on dilute dispersions in ethanol at a volume fraction of about 5×10^{-5}. Millipore filters were used to remove dust from the suspensions. Static light scattering (SLS) was performed with a Fica-50 photometer using vertically polarized light ($\lambda = 436$, 546, and 678 nm). Particle form factors were analyzed under the Rayleigh–Gans–Debye approximation.[29] The particles were assumed to be spherical and to have a homogeneous refractive index difference with the solvent. Under these assumptions the optical particle radius (R_0) was obtained from a fit of the measured scattered intensity to the Rayleigh–Gans–Debye formfactor as a function of the scattering angle ϑ ($20° \leqslant \vartheta \leqslant 150°$). Intensities at low angles did not show any sign of clustered particles.

Dynamic light scattering (DLS) results were obtained using an argon laser (Spectra Physics Series 2000) operating at 488.0 and 514.5 nm and a krypton laser (Spectra Physics model 2020) operating at 647.1 nm. To avoid convection due to absorption by the bleachable particles, the fluorescent spheres were measured at the non adsorbing wavelength 647.1 nm. Auto correlation functions were measured with a Malvern Multibit K7052 128 point correlator. Diffusion coefficients were obtained from a second order cumulant fit using auto correlation functions obtained from scattering angles between 35° and 140°.[30] The Stokes–Einstein relation Eqs. (6) and (9) was used to determine the hydrodynamic

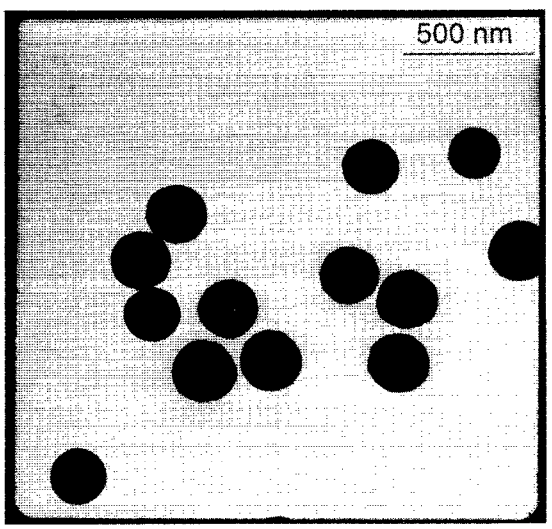

FIG. 2. Transmission electron micrograph of the charged spheres.

TABLE I. Particle radii.

Radii (nm)	HS	CS
TEM		
$\langle R \rangle$ (σ)	133 (5%)	122 (6%)
SLS[a]		
R_0	160 ± 1	139 ± 1
DLS		
R_H	159 ± 1	141 ± 1

[a] Optical radius determined in ethanol.

radius R_H. Diffusion coefficients were found to be independent of the scattering angle and the normalized second cumulants were smaller than 0.05 indicating unclustered monodisperse particles.

In the Stokes–Einstein relation Eqs. (6) and (9), the shear viscosity of the solvent appears. For the concentrations of LiCl in DMF exceeding 0.01 M the solvent shear viscosity was found to increase significantly above the value of pure DMF. A thermostatted Ubbelohde capillary viscosimeter (Schot–Gerate, GmbH) was used to determine the viscosity of LiCl solutions in DMF at 25.00 ± 0.01 °C as a function of the concentration LiCl. The measured viscosities are in good agreement with literature values.[31] As an indication, the viscosity, relative to pure DMF, for 0.050 M LiCl was found to be 1.070.

The different experimental radii are presented in Table I. As is almost always found in the characterization of larger (>20 nm) silica spheres, the TEM radius is systematically smaller than the optical and hydrodynamic radius. As has been put forward before, this is probably caused by the intensity of the electron beam and/or the high vacuum. However, the *relative* standard deviation σ can be measured quite accurately and is difficult to obtain otherwise. Given the relatively small polydispersity, it is possible to estimate that the hydrodynamic and optical radii, R_H and R_0, will be 2% larger than $\langle R \rangle$.[4(b)] These differences are the result of the fact that different moments of the particle size distribution are obtained with the different experimental techniques. FRAP results for D_S^L are weighted with the mobility of the spheres ($\propto R$), whereas DLS results for D_S^L are weighted with the squared particle volume ($\propto R^6$). DLS is therefore more sensitive to polydispersity than FRAP. It is clear that for the polydispersities of the systems studied here the effect of polydispersity on the experimentally obtained FRAP results for D_S^L will be small. The influence of polydispersity on the (self) diffusion process in concentrated dispersions is of course a different story.

2. Particle charges and Debye lengths

Electrophoretic measurements were made on the charged spheres (CS) dispersed in DMF with different concentrations of LiCl. The Pen Kem 3000 (Pen Kem Inc., New York) was used to determine the conductivity and mobility. Surface potentials were calculated by the procedure given in.[12] Volume fractions were close to 0.001.

Double layer characteristics are presented in Table II. The specific conductivities of the different LiCl concentrations in DMF are somewhat smaller than literature values.[32] This is probably caused by slight contaminations with water, since no care was taken to work under a dry atmosphere. The effects of (trace) amounts of water are described and discussed in Ref. 33. At higher concentrations the dissociation of LiCl is not complete anymore. For example, for 0.01 M the dissociation constant is 0.88. *For the values of κ given in Table II nonideality and dissociation effects were taken into account.*

The zeta potential ζ, as determined from electrophoretic mobilities, is the potential at the surface of shear. This imaginary surface is normally considered to lie close to the solid surface of a particle, within which the fluid is stationary. The absolute value of the surface potential, ψ_0, is generally smaller that the ζ potential. However, for the particles studied here we feel it is a justified first approximation to equal $\zeta = \psi_0$. This assumption is based on the nature of the surface and the origin of the charge. The surface charge is the result of dissociation of two kinds of chemical groups: silanol groups, which are located close to the silica surface, and carboxylic groups on the FITC molecules, which are coupled to aminopropyl moieties that are grafted onto the silica surface. The shear plane lies probably somewhere inside the thin grafted layer of aminopropyl groups, so that it seems appropriate to set ζ equal to ψ_0.

A further consequence of the dissociation of different surface groups is that for the dependence of the surface potential on the concentration of the potential determining ion, H^+, no Nernst-type equation holds. The surface potential is not fixed for a constant $[H^+]$, but is also depending on indifferent electrolyte concentrations through their effect on

TABLE II. Electrophoresis results: double layer repulsion characteristics.

LiCl[a] (M)	Conductivity (S/m)	κa	mobility $[10^{-8}\ m^2/(Vs)]$	Ψ_0 (mV)	Q (mC/m^2)
1.76×10^{-5}	1.84×10^{-4}	2.82	−2.14		
2.68×10^{-4}	2.05×10^{-3}	11.0	−1.89	−66	−2.3
2.38×10^{-3}	1.63×10^{-2}	32.8	−2.07	−59	−5.7
1.05×10^{-2}	6.26×10^{-2}	69.0	−1.86	−49	−9.1

[a] These values are concentrations of dissociated LiCl.

κ. The contribution of the carboxylate groups could be described with a site-dissociation model and the oxide surface with a more complex site-dissociation–ion-binding model.[12] Since, however, no values for the dissociation constants of the carboxylate and silanol groups in DMF are available, no quantitative calculations can be done in order to predict the experimental results in Table II. The trends that can be found in Table II are, however, in accordance with those given in the literature.[12,33]

The mobility of the CS in DMF *without added indifferent electrolyte* has not been used to calculate a surface potential. The concentration of LiCl, for the sample without added LiCl, given in Table II, is calculated assuming that the conductivity is due to Li^+ and Cl^- ions and should be considered merely as an order of magnitude. The ions really giving rise to that conductivity are not exactly known. Among the contributing ions are certainly the counter ions of the dissociated surface groups; for these low concentrations there are certainly also contaminations that contribute significantly to the conductivity. Given the fact that for κa values between two and ten corrections for relaxation effects are large, a surface potential without added LiCl can not be given.

Diffusion coefficients D_0 were measured for five LiCl concentrations ranging from no added salt to 0.5 M LiCl. All the DLS results were independent of the scattering angle and gave D_0 values that were the same within experimental uncertainties for even the highest concentration of LiCl. This clearly demonstrates that there is no electrolyte friction contribution to D_0 ($= 1.96\,\mu m^2/s$).

Another conclusion that can be drawn from our measurements of D_0 as a function of indifferent electrolyte concentration is about the Hamaker constant A. Because there was no clustering at concentrations of LiCl of 0.5 M, the critical coagulation concentration (ccc) must be even higher. If we take the ccc as the concentration at which the DLVO potential barrier, Eq. (1), disappears, an upper limit for the value of A can be calculated.[11] This calculation gives a value of $A \leqslant 0.5$ kT, which is very small. The reason for this small value is probably the almost perfect matching of the refractive index of the particle and the solvent. It is also possible that some kind of solvatation layer is responsible for this unusual stability. This is for instance the explanation for the stability of silica in water close to the point of zero charge.[34]

IV. LONG-TIME SELF-DIFFUSION COEFFICIENTS

In this section we will present FRAP results on D_S^L as a function of the hard-core volume fraction of the charged and hard spheres, of which the characteristics were discussed in the previous section.

A. Experimental

Volume fractions are calculated using a specific weight of 1.75 g/ml for the charged spheres and 1.79 g/ml for the hard spheres. These particle densities were measured by drying a known volume of a concentrated dispersion in a pure solvent under nitrogen for 24 h at 100 °C, and weighing the residue. The higher volume fractions were prepared by centrifuging a dispersion of precisely known weight/weight concentration (corresponding to a volume fraction of about 15%), and after removal of some of the supernatant, redispersing and weighing, the volume fraction was calculated from the above given particle density. Different concentrations of LiCl were made by adding a weighted amount of concentrated LiCl solution in DMF followed by rapid homogenization. Volume fractions are corrected for the addition of LiCl solution. LiCl concentrations always refer, by definition, to moles of LiCl per dm^3 of suspension. *The LiCl concentration in the solvent, that should be used in any interaction potential calculation, is thus $1/(1-\phi)$ times larger than the given concentrations*, where ϕ is the volume fraction of colloidal particles.

The specific weight determined as described above does not take the layer of immobilized solvent molecules in between the alkane molecules on the surface into account. For a dynamic description of the particle motions this immobilized layer of solvent molecules should be considered as part of it. An increase of the hydrodynamic radius of a particle of 150 to 151 nm causes already an increase in the volume fraction of a few percent. However, the HS used in this work showed at high volume fractions the crystallization behavior that is expected for hard spheres, including homogeneous, heterogeneous, and settling crystallization.[35] The fluid-crystalline coexistence concentrations were found to be very close to the theoretical crystallization and melting volume fractions of $\phi = 0.494$ and 0.55, respectively. From these findings we conclude that the determined density is, perhaps somewhat fortunate, quite close to its thermodynamic value.

The cuvettes that were used in the FRAP setup are flat glass capillaries (width 2 mm, Vitro Dynamics, Inc. Rockaway, N.J.) of thickness 50, 100, and 200 μm. The temperature was 23–27 °C. All D_S^L values given, are corrected to 25.0 °C for differences in the solvent viscosity.

For all CS samples the fringe spacing is 31.4 μm. Because the FITC groups are here on the outer surface of the silica spheres and determine some of its charge, it was checked that bleaching did not change the interaction potential. At a volume fraction of 24.1%, without added LiCl, the same spot was bleached repeatedly until the total fluorescent intensity was less than half its original value. The measured D_S^L was found to be the same before and after this bleaching procedure. This most probably means that the photochemical reaction does not change the charge of the FITC molecule. The interaction potential is not significantly changed due to bleaching.

The HS particles were measured at fringe spacings of 21.7, 26.7, or 36.6 μm.

B. Results

Figure 3 shows typical signal decay curves. These are measurements on three different concentrations of charged spheres. The drawn curves are single exponential fits. These experiments are thus indeed seen to be described by Eq. (19), as far as the time dependence is concerned. Notice that measuring times are as long as about 10 min. The q dependence of the decay rate $\tau = 1/D_S^L \cdot q^2$ of S in Eq. (19) is veri-

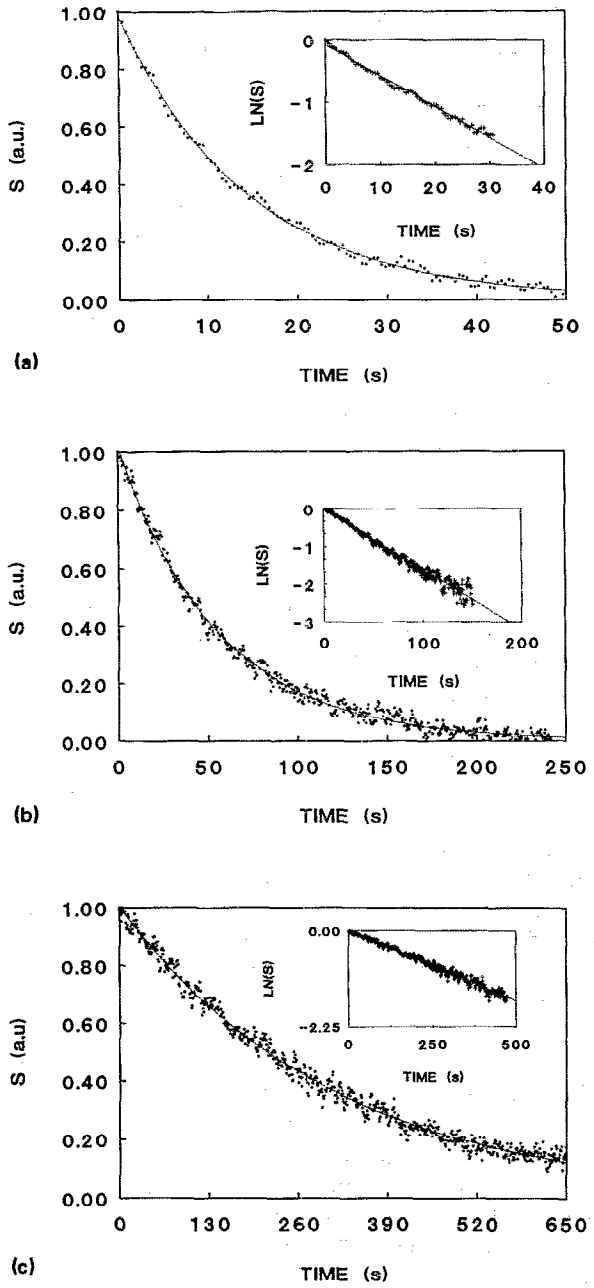

FIG. 3. Modulation envelope of the intensity (S) as a function of time after the bleaching of the charged sphere system. The insert shows a semilogarithmic plot of the same data. Drawn curves are single exponential fits to the data. (a) $\phi = 1.4\%$, $D_S^L = 1.87 \pm 0.19$ $\mu m^2/s$; (b) $\phi = 16.8\%$, $D_S^L = 0.39 \pm 0.07\,\mu m^2/s$; (c) $\phi = 22.7\%$, $D_S^L = 0.08 \pm 0.02\,\mu m^2/s$.

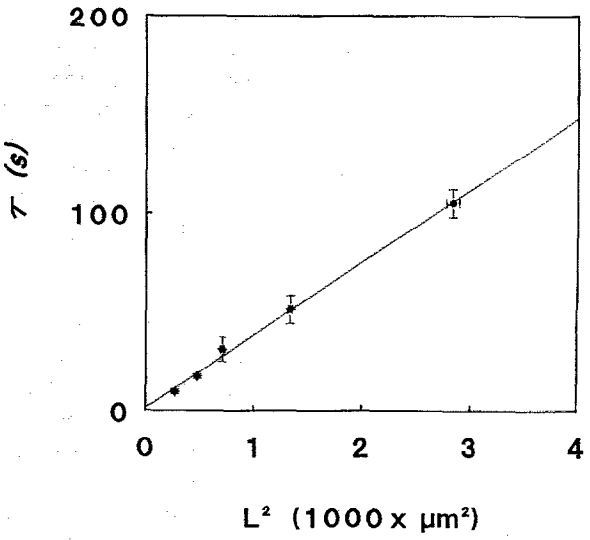

FIG. 4. Decay times (τ) of the hard spheres system in cyclohexane at $\phi = 24.1\%$ as a function of the square of the interference spacing (L^2). L is related to the wavevector q as $L = 2\pi/q$.

fied in Fig. 4. In this figure L is the fringe spacing, which is related to q as $L = 2\pi/q$. These measurements were performed on the hard sphere system.

1. Hard spheres

In Fig. 5 the D_S^L values for the stearyl silica spheres in cyclohexane are given (▲) together with results from others. For D_0 we used the value as determined by dynamic light scattering in cyclohexane ($= 1.60\,\mu m^2/s$). The hard-sphere character of the stearyl silica particles in this solvent has been discussed in several studies (for instance, Refs. 14–16). *If* the long-range Van der Waals forces can be neglected and the thin layers are repulsive at contact during collisions of the particles, hard-sphere behavior is to be expected. Although the DLS measurements are difficult with a tracer system, several groups have reported on D_S^L as a function of ϕ for comparable hard-sphere-like particles.[3–6] As far as we know no D_S^L coefficients for hard spheres have been measured with other techniques. Included in the figure are mea-

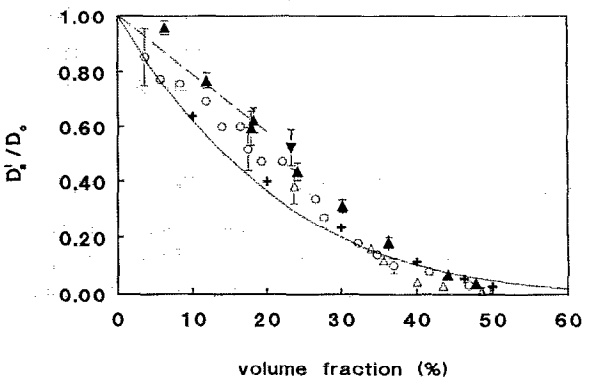

FIG. 5. Long-time self-diffusion of hard spheres in cyclohexane as function of the volume fraction ϕ (▲); (○) Ref. 5, (△) Ref. 6, (+) values given by Eq. (15), using simulation results from Ref. 24 for D_S^H and experimental results for D_S^S from Ref. 18, (▼) see the text. The drawn curve represents Eq. (24) and the dashed curve is the first order in ϕ result, Eq. (14).

surements that represent the most extensive DLS measurements on a quite monodisperse tracer system (○, from Ref. 5) and the first measurements of D_S^L at high volume fractions for the stearyl silica system △, from Ref. 6(a). The low volume fraction behavior of D_S^L has been analyzed by Kops-Werkhoven *et al.*[6(b)] The first order volume fraction coefficient found there is -2.7 ± 0.3 which is a bit high, but still quite close to the exact result, Eq. (14). Also included in Fig. 5 are the predictions of the proposal from Medina-Noyola,[25] Eq. (15), using the simulated results from Cichocki and Hinsen[24] for D_S^H and the results from Beenakker and Mazur[18] for D_S^S/D_0 (+).

The D_S^L values obtained in this work and from Refs. 5 and 6 are almost completely in each others error range. We should mention that some literature values are omitted for clarity from Fig. 5 (like those from Refs. 4 and 3) which show less agreement for volume fractions smaller than 20%. The agreement for the higher volume fractions is much better. As suggested by Van Megen and Underwood[5(a)] it is possible that these differences are caused by the higher polydispersities of these systems as compared to that of Ref. 5(a). Although the polydispersity of particles in this work is clearly higher than for the system used in Ref. 5(a) (2%), the measurement of D_S^L with FRAP is much less influenced by it, as was already discussed in the previous section. Unfortunately, the low fluorescent intensities measured with the volume fractions less than 5% make conclusions about the first order ϕ dependence, Eq. (14), speculative.

A D_S^L value obtained from FRAP measurements using the fluorescent HS particles as a tracer is also included in Fig. 5 (▼). The host particles have a radius of 140 nm which is different from those of the tracer particles, 160 nm. It does show that true tracer measurements are possible.

Equation (15) seems to describe the results for the higher volume fractions reasonably well. This suggests that for highly concentrated dispersions the trajectories that a tracer particle traverses over long distances, are not much affected by hydrodynamic interactions. Hydrodynamics is than decoupled from the effects of the direct interactions and can in a first approximation be described by D_S^S. However, a fortuitous cancellation of opposing effects can at this moment not be excluded.

2. Charged spheres

Figure 3 shows some of the fluorescence decay signals Eq. (19) of the charged system without added LiCl for different volume fractions. The figures demonstrate the exponential character of the decay process and the possibility of the FRAP method to measure a wide range of diffusion coefficients, including very slow processes. The effect of adding indifferent electrolyte LiCl on D_S^L for two fixed volume fractions is depicted in Fig. 6. Actually, the measurements were not done at fixed ϕ. Because of the addition of LiCl, there is a change of about 1% in the volume fractions as D_S^L was measured. The values presented in Fig. 6 were interpolated to $\phi = 13.0\%$ and 23.0% with the help of Fig. 7.

The results in Fig. 6 are qualitatively understood by looking at Table II. At first the concentration of LiCl is so

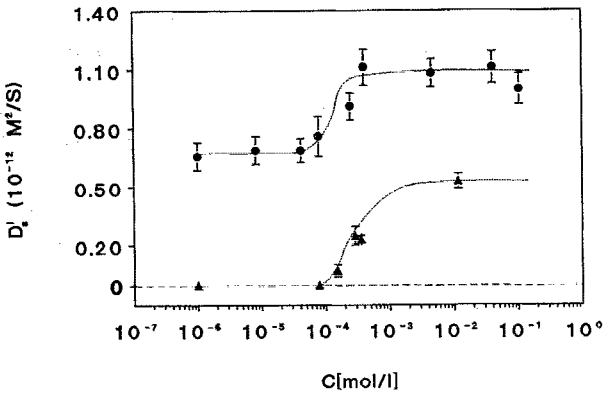

FIG. 6. Effect of the concentration of LiCl (c) on D_S^L for the charged spheres at two fixed volume fractions: (●) $\phi = 13\%$, (▲) $\phi = 23\%$. The drawn curves are to guide the eye.

low, that its effects on κ can be neglected. From the surface charge on the spheres, the concentration of counter ions in DMF can be calculated. This gives for the volume fraction 13.0% a value of 8×10^{-5} M and for $\phi = 23.0\%$, 1.4×10^{-4} M. These values are consistent with Fig. 6 since a double layer thickness decrease will become apparent at concentrations comparable to the concentration of ions already present in the dispersion. At concentrations above 10^{-2} M LiCl the double layer thickness is on the order of nm's and a further increase in D_S^L as a result of decreasing direct interactions is not possible. For these high salt concentrations, corrections for the dependence of the solvent viscosity on the

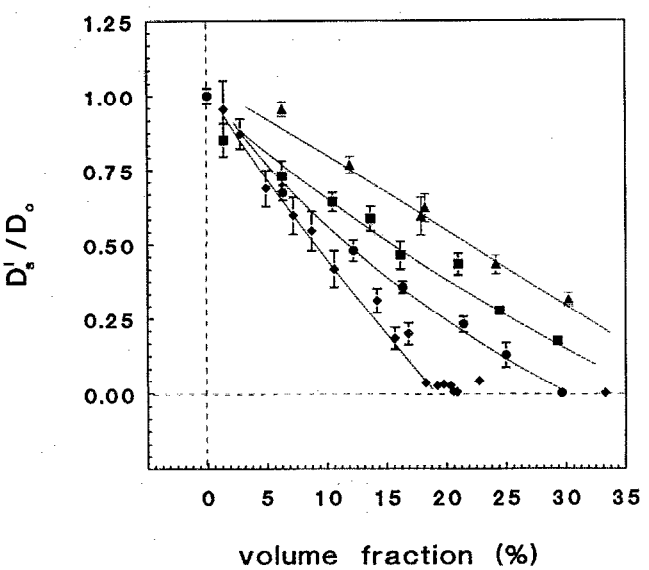

FIG. 7. Long-time self-diffusion as a function of volume fraction and indifferent electrolyte concentration LiCl in DMF: (■) no salt added, (●) 2.8×10^{-4} M LiCl, (◆) 1.2×10^{-2} M LiCl. (▲) are the hard sphere results, which are also plotted in Fig. 5. The drawn curves are to guide the eye.

LiCl concentration were made. Figure 6 shows the melting of the crystal phase for the large volume fraction as the LiCl concentration is increased. Here no diffusion could be measured for the two lowest concentrations of LiCl and crystallites were visible in the cuvettes. In view of these results it was decided to study D_S^L as a function of ϕ without added salt, with 2.8×10^{-4} M LiCl (partly compressed double layer) and for 1.2×10^{-2} M (almost completely depressed repulsion).

Figure 7 clearly demonstrates the hindering effects of the direct repulsive interactions on the long-time self-diffusion coefficient. Here D_S^L is, again, scaled on the diffusion coefficient at "infinite" dilution ($D_0 = 1.96\ \mu m^2/s$). Qualitatively these results have also been found with FRS by Dozier *et al.*[8] They used highly charged latex spheres of about 20 nm radius. At a volume fraction of 8%, D_S^L was almost zero. However, with such small particles electrofriction should also be considered to play a role. They did not mention this effect on D_S^L. With the same kind of particles Gorti *et al.*[9] reported FRAP measurements where the decrease in D_S^L as compared to D_0 was considered to be completely caused by this relaxation delay of the double layer.

In the range of volume fractions studied by us the spheres with 1.2×10^{-2} M salt did not crystallize. The two other charged sphere systems did show crystallization, resulting in a zero value for D_S^L. In the crystal phase no diffusion could be detected. In order to determine whether D_S^L approaches its zero value slowly and continuously or with a sudden decrease, the charged spheres without added salt were investigated in more detail around $\phi = 20\%$. No discontinuity in D_S^L could be detected. In Ref. 8 a "jumplike" change of D_S^L was observed upon melting of the colloidal crystal phase. The reason for this apparent discrepancy may be, that in the system of Dozier *et al.* both the Debye screening length and the surface charge of the particles were significantly changed upon addition of HCl to melt the crystals. In our study only the volume fraction was changed. The jumplike increase of D_S^L reported by Dozier may be the result of the extreme sensitivity of D_S^L on changes in the interaction potential.

To our surprise a diffusion process was observed, reproducibly, at $\phi = 22.7\%$ while measurements at lower concentration did not show any fluorescence relaxation. A speculative explanation is, that the nucleation/crystallization rates have decreased in comparison with those at the somewhat lower volume fractions so that the measurements were actually made in a non equilibrium fluid phase. Another possible explanation has to do with the inter particle potential. As was seen in Fig. 6 a crystal suddenly starts melting if the double layer thickness is decreased. With increasing volume fraction the volume available to the counter ions in DMF decreases, so that their concentration increases. This small increase in counter ion concentration could have shifted the crystallization point. A third explanation could be, that diffusion of particles along grain boundaries is measured. However, it is clear that further work is necessary in the neighborhood of the crystallization volume fraction to clarify this point.

V. RESCALING AND TENTATIVE COMPARISONS

In view of the theoretical results for the first order ϕ behavior and the success of the assumptions leading to Eq. (15) for the higher volume fractions, it would be interesting to see what the effects are of hydrodynamic interactions in the charged systems. To first approximation, a comparison can be made when the effects of the repulsion are represented by an increase in the hard-core interaction radius of the particles just as was done in the calculations of Cichocki and Felderhof.[22] Only the two curves with added salt can be rescaled, since the identity and concentration of ions in the pure solvent are unknown. The problem in the proposed rescaling is to find a procedure to determine the increase of the diameter. Unfortunately, the particles in DMF, although quite well matched, scattered too much for an experimental determination of the structure factor. Furthermore, although the analytical mean spherical approximation is known to describe the structure of weakly charged systems like ours very well, the model surface charge often differs from the experimentally determined value. A rescaling procedure based on structure factor considerations is therefore not feasible. We have chosen to use a thermodynamic rescaling argument instead. An effective hard-core radius is defined, such that the second virial coefficient of the corresponding hard sphere system equals that of the charged sphere system (see Ref. 36 for a similar procedure). The increase in radius $(b-a)$ is then given by

$$b^3 - a^3 = \int_2^\infty \frac{3}{8}\mathbf{r}^2[1-\exp\{-V(r)/kT\}]dr. \quad (20)$$

The results presented in Sec. III have made it clear that only the double layer repulsion needs to be considered in the interparticle potential $V(r)$, because the Hamaker constant is very small. The scaling factor $(b/a)^3$ by which the volume fraction of the core of the particles should be multiplied can now be evaluated using the results for the double layer thickness and surface potential given in Table II. Since the LiCl concentration in the solvent that should be used in an interaction potential calculation is $1/(1-\phi)$ times larger than the given concentration in Table II, b/a varies with the volume fraction ϕ. For the LiCl concentration of 1.2×10^{-2} M the double layer was already so far compressed that these effects were unimportant and the scaling factor is 1.1 for all the volume fractions. The factor $(b/a)^3$ for the 2.8×10^{-4} M LiCl system ranged from 1.8 to 2.0. To get an idea of the sensitivity of the rescaling factor to the scaling argument that is used, we also considered a different scaling procedure. The rescaled radius in this procedure is chosen as the distance were the double layer repulsion reaches a value of $1\ kT$ or $2\ kT$. This scaling gives factors 2.0 for kT and 1.9 for $2\ kT$, for the 2.8×10^{-4} M LiCl system for which the "thermodynamic scaling" procedure gives 2.0. The three rescaling procedures thus give very similar results for the rescaled radii.

The rescaled curves are given in Fig. 8 together with the hard sphere values and the simulation results for the hard spheres without hydrodynamic interactions. As expected the particles with the most compressed double layer (□) are closest to the hard sphere values (△), because hydrodynamics is almost equally important in both cases. The first or-

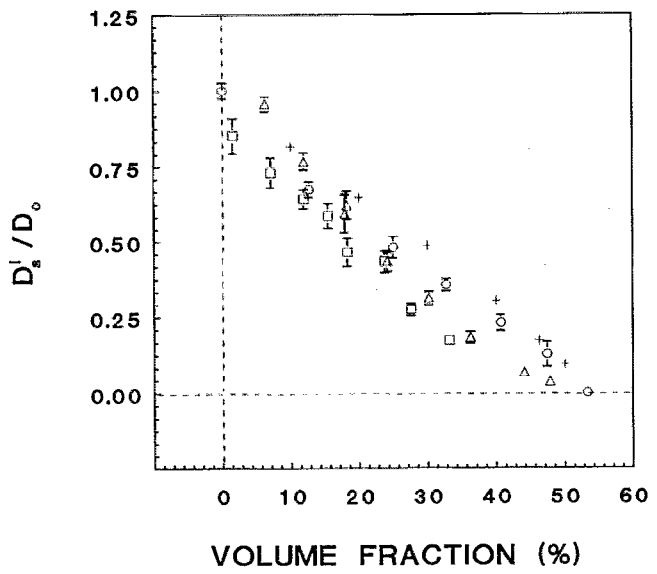

FIG. 8. D_S^L as a function of the rescaled volume fraction: (○) 2.8×10^{-4} M LiCl in DMF; (□) 1.2×10^{-2} M LiCl in DMF, (△) hard spheres in cyclohexane; and (+) simulation results without hydrodynamic interactions Ref. (24).

der in ϕ coefficient describing the difference of D_S^L from D_0 for $(b/a)^3\simeq 2$ [the not so compressed double layer (○), $(b/a)\simeq 1.3$, see Sec. II B] is equal to -1.26; only 60% of the hard-sphere value -2.1. Such a large difference in slope between our rescaled charged spheres and hard sphere results as a function of ϕ is not found experimentally for any range in volume fractions. This indicates that for higher volume fractions the effects of the hydrodynamics *on the direct-interaction hindering*, i.e., the modification of the pair distribution function, of the diffusion is (much) less important than for low volume fractions. The rescaled results for this lower concentration of LiCl (0) are as expected closer to the simulation results from Ref. 24 (+) where hydrodynamics is neglected. Furthermore there is a large difference between the result with (△) and without (+) hydrodynamic interactions at larger volume fractions. It thus seems that hydrodynamic interactions are of significant importance. The comparison of hard sphere results with Medina-Noyola's theory, as discussed before, shows that these hydrodynamic effects are probably accounted for through its effect on D_S^S in Eq. (15).

An analytical expression for D_S^L for hard spheres as a function of the volume fraction ϕ on the basis of Eq. (15) may be constructed as follows. The long-time self-diffusion coefficient for hard spheres without hydrodynamic interactions, D_S^H, is obtained by formally replacing the pair-correlation function in the two particle result for D_S^H [37] by a more accurate function,[38]

$$D_S^H=\frac{D_0}{1+2\phi\chi}, \tag{21}$$

where χ is the contact value of the pair-correlation function. In the Percus–Yevick approximation χ is given by

$$\chi=\frac{1+(1/2)\phi}{(1-\phi)^2}. \tag{22}$$

Next, the short-time self-diffusion coefficient as a function of ϕ has been given in a mean-field approximation by Mazur and Geigenmüller,[19]

$$D_S^S=D_0\cdot\frac{1-\phi}{1+(3/2)\phi}. \tag{23}$$

Using Eqs. (21)–(23) together with Medina-Noyola's Eq. (15) yields

$$D_S^L=D_0\cdot\frac{(1-\phi)^3}{[1+(3/2)\phi+2\phi^2+3\phi^3]}. \tag{24}$$

This relation describes the hard-sphere data for $\phi\geqslant 0.2$ reasonably well as can be seen from Fig. 5 [the full curve is Eq. (24)]. Because Eq. (21) is a quite good approximation for D_S^H [38] and Eq. (23) describes the experimental and theoretical D_S^S quite well, the points calculated with Eq. (15), using simulation results from Ref. 24 for D_S^H and experimental results for D_S^S from Ref. 18 lie almost completely on the curve given by Eq. (24).

Another interesting comparison can be made. It is known that there is a connection between a liquid's long-time self-diffusion coefficient and its low shear-rate low-frequency viscosity. Experimentally, the Stokes–Einstein relation has been found to hold for molecules in liquids at high densities, although sometimes a small density dependence on the molecular radius is needed (see the references in Ref. 39). Theoretically one has tried to provide a basis for such findings.[39,40]

The idea to use the Stokes–Einstein relation to obtain the long-time self-diffusion coefficient for colloids through the use of the low shear-rate viscosity (η) instead of the solvent viscosity (η_0) has been used before.[6(a),17] Recently, accurate shear viscosities for hard sphere stearyl silicas have been reported.[41] In Fig. 9 we present these low shear data as $1/\eta_R=\eta_0/\eta$. The reciprocal relative viscosity η_R seems to describe the D_S^L data for all volume fractions quite well.

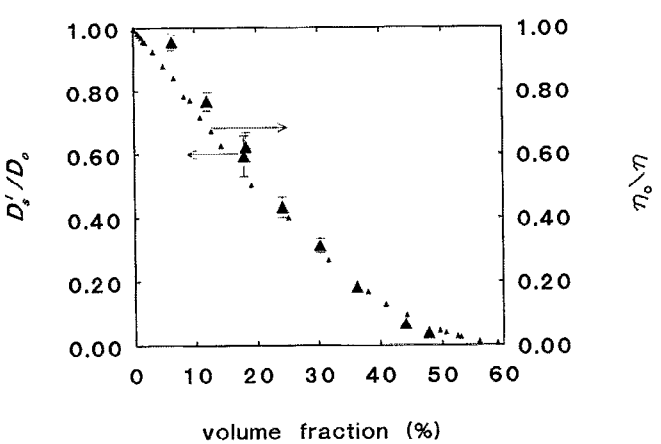

FIG. 9. D_S^L of the hard-sphere system (▲) compared to the reciprocal relative viscosity (Ref. 37), η_0/η (▲).

The first order in volume fraction coefficient for D_S^L is -2.1 for hard spheres [see Eq. (14)], whereas for η_0/η this is -2.5, independent of the kind of interaction potential that is considered. From Fig. 7 it is clear that the D_S^L coefficient significantly changes as the interaction potential is altered. Thus, at least for the low volume fractions, no (approximate) agreement between D_S^L and η_0/η is expected in general. Only for hard spheres these two quantities (approximately) coincide. Higher orders in volume fraction coefficients, however, do become significant already at small volume fractions for the shear viscosity. It may be that the coincidence of D_S^L and η_0/η at larger volume fractions is also only true for hard spheres. Further study on charged systems will be necessary to clarify this issue.

VI. SUMMARY AND CONCLUDING REMARKS

The long-time self-diffusion coefficient D_S^L is more rapidly decreasing with the colloid concentration as the Debye screening length of the repulsive interaction potential is increased, and goes to zero, probably, at the melting concentration. The approach of D_S^L towards zero is continuous (to within experimental error), indicating that D_S^L in the coexisting fluid phase is very small. If this would not be the case, a jump of the experimental D_S^L from its finite value in the coexisting fluid phase to its zero value in the crystalline phase would have been found.

The hard sphere results for D_S^L as a function of the volume fraction ϕ are reasonably well described at larger volume fractions ($\geqslant 0.2$) by the approximate formula of Medina-Noyola, Eq. (15). Although the initial slope of the D_S^L vs ϕ, as predicted by this equation is almost a factor 2 off, the higher order terms in ϕ are described more accurately. It would be interesting to analyze the D_S^L results also for the charged system with Medina-Noyla's theory; the main thing to be done here is to calculate or simulate D_S^H. If Eq. (15) also predicts the correct behavior for long-time self-diffusion for charged systems, it is likely that the assumption to include all hydrodynamic effects in a term represented by D_S^S seems justified. Contrary to what exact calculations show for low volume fractions, this would mean that for higher volume fractions the contribution from direct interactions and distortion of the pair correlation function are not influenced much by hydrodynamic interactions.

It was found that for the long-time self-diffusion of the charged spheres, rescaling of the additional repulsive interaction potential to an effective hard sphere seems to work, at least for the range of potentials used here. Rescaling the volume fraction of the charged spheres with a small Debye length maps the D_S^L vs ϕ curve just above the curve for hard spheres; the small difference may be attributed to the smaller effect of hydrodynamic interactions for the charged spheres. Rescaling of the charged spheres with a large Debye length maps D_S^L vs ϕ just below hard sphere (simulation) results without hydrodynamics. The small difference may be attributed to the effect of hydrodynamic interactions still present in the charged system.

Hydrodynamic interactions are important for any description of long-time self-diffusion. At the larger volume fractions the difference between D_S^L values with and without hydrodynamic interactions may exceed 100%.

For hard spheres, to within experimental error, the Stokes–Einstein relation for D_S^L holds when the (zero frequency and zero shear-rate) suspension viscosity is used. The low volume fraction agreement is fortuitous. Further study on charged systems is necessary to assess the generality of this relation.

The particles with the fluorescent labels build into the silica core allow for FRAP studies in any environment where a proper surface treatment of these particles renders a stable system. The signal to noise ratio as compared to the measurements presented in this work can be significantly increased by the use of particle cores where the fluorescent molecules are not only located in a thin layer, but are distributed throughout the whole volume of the particle. We have recently been able to synthesize such particles.[10] This opens the way to studies of long-time self-diffusion for various interaction potentials in various systems.

ACKNOWLEDGMENTS

We are grateful to Dr. P. Mast and Dr. F. Marsen (DSM-Research, Geleen, The Netherlands) for the electrophoresis measurements. We appreciated the stimulating discussions with Professor A. Vrij and Professor H. N. W. Lekkerkerker and their critical reading of the manuscript. This work was supported by the Netherlands Foundation for Chemical Research (SON) with financial aid from the Netherlands Organization for Scientific Research (NWO).

[1] A. Einstein, *Investigations on the Theory of the Brownian Motion* (Dover, New York, 1956).
[2] J. Perrin, *Brownian Motion and Molecular Reality* (Taylor and Francis, London, 1910).
[3] R. H. Ottewill and N. St. J. Williams, Nature (London) **325**, 232 (1987).
[4] (a) A. van Veluwen and H. N. W. Lekkerkerker, Phys. Rev. A **38**, 3758 (1988); (b) A. van Veluwen, H. N. W. Lekkerkerker, C. G. De Kruif, and A. Vrij, J. Chem. Phys. **89**, 2810 (1988).
[5] (a) W. van Megen and S. M. Underwood, J. Chem. Phys. **91**, 552 (1989); (b) W. van Megen and S. M. Underwood, Langmuir **6**, 35 (1990).
[6] (a) M. M. Kops-Werkhoven and H. M. Fijnaut, J. Chem. Phys. **77**, 2242 (1982); (b) M. M. Kops-Werkhoven, C. Pathmamanoharan, A. Vrij, and H. M. Fijnaut, **77**, 5913 (1982).
[7] A. P. Philipse and A. Vrij, J. Chem. Phys. **88**, 6459 (1988).
[8] W. D. Dozier, Lindsay, and P. M. Chaikin, J. Phys. (Paris), **3**, c3 (1985).
[9] S. Gorti, L. Plank, and B. R. Ware, J. Chem. Phys. **81**, 909 (1984).
[10] A. van Blaaderen and A. Vrij (submitted).
[11] E. J. W. Verwey and J. Th. G. Overbeek, *Theory of the Stability of Lyophobic Colloid* (Elsevier, New York, 1948).
[12] R. J. Hunter, *Zeta Potential in Colloid Science* (Academic, London, 1981).
[13] J. W. Jansen, C. G. de Kruif, and A. Vrij, J. Colloid Interface Sci. **114**, 471 (1986).
[14] C. G. de Kruif, J. W. Jansen, and A. Vrij, *Physics of Complex and Supermolecular Fluids* (Wiley, New York, 1987).
[15] C. G. de Kruif, W. J. Briels, R. P. May, and A. Vrij, Langmuir **4**, 668 (1988).
[16] (a) A. K. van Helden and A. Vrij, J. Colloid Interface Sci. **78**, 312 (1980), (b) A. K. van Helden, J. W. Jansen, and A. Vrij, *ibid.* **81**, 354 (1981).
[17] P. N. Pusey, *Liquids, Freezing and the Glass Transition*, edited by D. Levesque, J.-P. Hansen, and J. Zinn-Justin (Elsevier, Amsterdam, 1990).
[18] C. W. J. Beenakker and P. Mazur, Physica A **126**, 349 (1984).
[19] P. Mazur and U. Geigenmueller, Physica A **146**, 657 (1987).
[20] B. Cichocki and B. U. Felderhof, J. Chem. Phys. **89**, 3705 (1988).

[21]H. N. W. Lekkerkerker and J. K. G. Dhont, J. Chem. Phys. **80**, 5790 (1984).
[22]B. Cichocki and B. U. Felderhof, J. Chem. Phys. **94**, 556 (1991).
[23]W. van Megen and I. Snook, J. Chem. Soc., Faraday Trans. 2 **80**, 383 (1984).
[24]B. Cichocki and K. Hinsen, Physica A **166**, 473 (1990).
[25]M. Medina-Noyola, Phys. Rev. Lett. **60**, 2705 (1988).
[26]F. Lanni and B. R. Ware, Rev. Sci. Instrum. **53**, 905 (1982).
[27]J. Davoust, P. F. Devaux, and L. Leger, EMBO J. **1**, 1233 (1982).
[28]W. Stöber, A. Fink, and E. Bohn, J. Colloid Interface Sci. **26**, 62 (1968).
[29](a) M. Kerker, *Scattering of Light and Other Electromagnetic Radiation* (Academic, New York, 1969); (b) C. F. Bohren and D. R. Huffman, *Absorption and Scattering of Light by Small Particles* (Wiley, New York, 1983).
[30]*Dynamic Light Scattering: Applications of Photon Correlation Spectroscopy*, edited by R. Pecora (Plenum, New York, 1985).
[31]P. Haldar and D. K. Majumdar, Z. Phys. Chem. Neue Folge **165**, 133 (1989).
[32]J. Prue and P. J. Sherrington, Trans. Faraday Soc. **57**, 1795 (1961).
[33]J. M. Kleijn, Colloid Surf. **51**, 371 (1990).
[34]R. K. Iler, *The Chemistry of Silica* (Wiley, New York, 1979).
[35]P. N. Pusey and W. Van Megen, Nature (London) **320**, 340 (1986).
[36]W. B. Russel, D. A. Saville, and W. R. Schowalter, *Colloidal Dispersions* (Cambridge University, Cambridge, 1989).
[37]B. J. Ackerson and L. Fleishman, J. Chem. Phys. **76**, 2675 (1982).
[38]G. Szamel and J. A. Leegwater, Phys. Rev. Lett. (submitted).
[39]R. Zwanzig, J. Chem. Phys. **79**, 4507 (1983).
[40]U. Balucani, R. Vallauri, and T. Gaskell, Ber. Bunsenges. Phys. Chem. **94**, 261 (1990).
[41]J. C. van der Werff and C. G. de Kruif, J. Rheol. **33**, 421 (1989).